The role of Light-Sheet microscopy in understanding early (pT1/2) colorectal cancer development.

By Hattie McCance

June 2019

Supervised by Professor Philip Quirke and Dr Scarlet Brockmoeller.

With special thanks to Gemma Hemmings, Georgia Mappa and Hayley Slaney for their laboratory assistance.

Contents

Introduction

Colorectal Cancer

Colorectal cancer (CRC) is the third most common malignant cancer in both sexes (2). In 2018 there were 1.8 million diagnoses worldwide (3).

This project will investigate the potential of a new technique capable of analysing the development and spread of early cancers (pT1 and pT2).

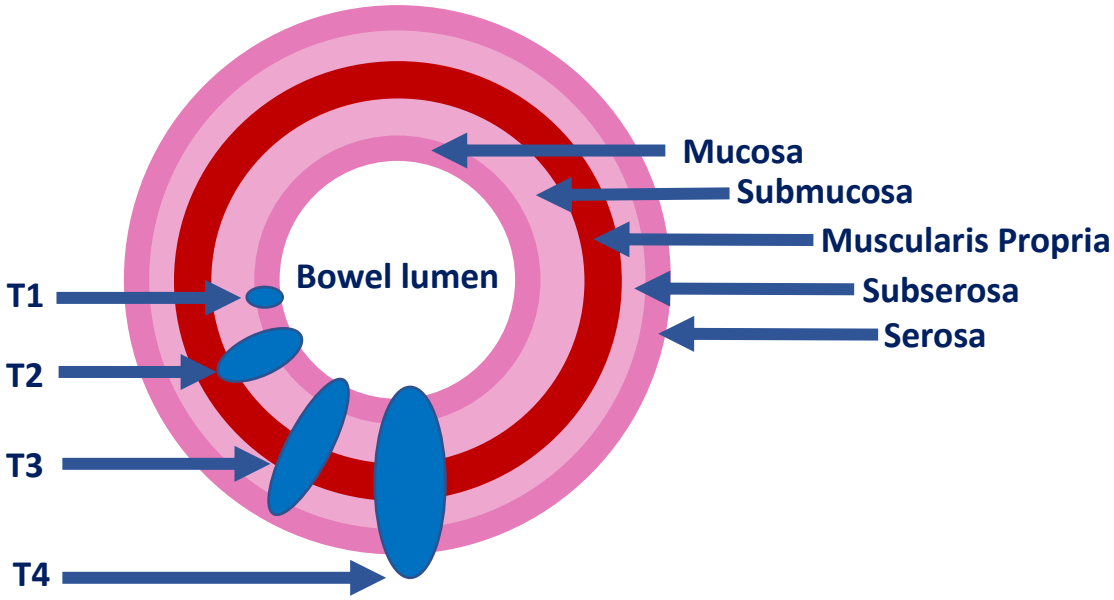

Figure 1: TNM staging.
Adapted from Cancer Research UK
(4)

Figure 1 shows the different invasion patterns seen by each pathological stage of tumour. T1 tumours only invade the submucosa of the bowel, T2 tumours invade into the muscularis propria, T3 tumours invade into the subserosa but not through the serosa of the bowel wall. T4 tumours have invaded through all layers of the bowel wall.

Currently all patients with pT2 CRC tumours, and 60% of patients with pT1 CRC undergo major surgery (5). At diagnosis only 5-10% of pT1 and 15-25% of pT2 cancers have lymph node metastases (LNM) (5). Local spread without LNM may be locally excised. There are currently no reliable clinical markers or risk stratification models used to predict LNM in CRC.

The bowel cancer screening program, introduced in 2006, has provided a new cohort of CRC patients who are detected with earlier stage disease (5). With better methods of predicting LNM these patients would be suitable for local excision of their tumour.

How can light-sheet microscopy solve problems of 3-dimensional (3D) imaging bowel tumours

Currently tumours are analysed in 2 dimensions (2D).

Better understanding of tumour morphology in 3D would allow better surgical techniques to be developed for tumour removal as well as better tumour stratification models (1).

Recent developments in digital pathology have allowed 3D reconstructed images to be made from stacked 2D images of normal tissue (6). Digital pathology is an expensive and labour-intensive method so is not viable for high throughput work.

Results seen in 3D exposed important new information about the microvasculature of the bowel wall. Previously, risk of tumour metastasis was thought to be determined by the lesion's depth of invasion. Toh et al. showed that area of submucosal invasion is a better parameter for metastatic risk using 3D reconstructed images (7).

This project aims to reproduce the model shown by Brown et al. using whole tissue imaging on the light-sheet microscope. This will provide cheaper and less labour-intensive 3D imaging than digital pathology and is the only current technique allowing whole tissue analysis.

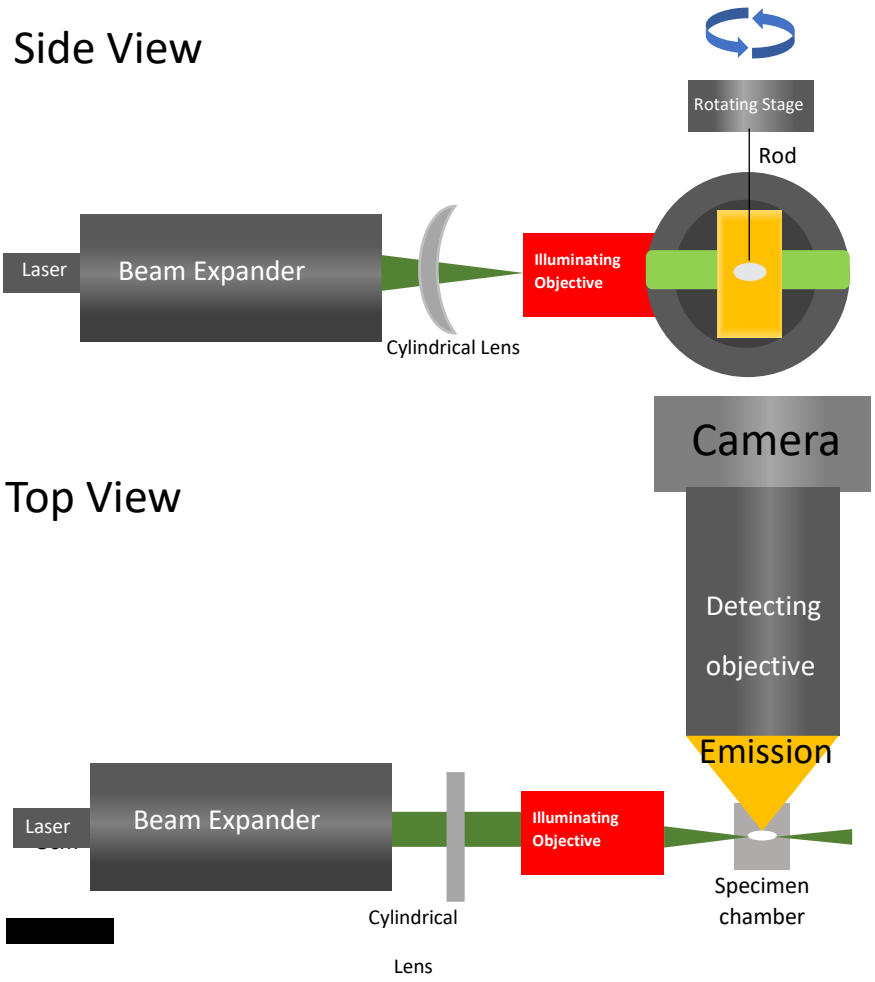

Figure 2: Components of the Light-sheet microscope.

Adapted from Light Sheet Fluorescence Microscopy: A review

(8)

This diagram shows the main components of a light-sheet microscope from two angles. A side view and a bird's eye view. The light-sheet itself is created by a laser, it is accurately aligned and expanded using a beam expander. A cylindrical lens forms the light-sheet (green beam) which is projected through an illuminating objective. The focal point (the thinnest portion of the light-sheet is positioned in the middle of the specimen chamber. This chamber is made of optically clear glass with an open top for specimen access. For cleared tissue the chamber contains clearing fluid (di-benzyl ether in the following experiments).

The specimen (illustrated by the white ellipsoid) is illuminated, by the light-sheet, one plane at a time. The emitted light (orange cone labelled emission) is collected by the microscope. The sample can be micro-positioned using rotating and translating stages (not shown).

The specimen is imaged along the x-axis to produce a well-focused complex image across the width of the specimen. By then moving the specimen in the z-axis (and obtaining another image), a stack of well-aligned, serial optical sections is obtained. This is known as a z-stack.

Aims:

1. Investigate the potential use of light-sheet microscopy on both normal and tumorous colorectal tissue. This includes optimisation of an optical clearing technique.
2. The secondary aim of the project will be to optimise CD31, D2:40 and cytokeratin staining for confocal and light-sheet microscopy.
3. To compare the efficacy of lectin staining compared with antibody staining.

Methods

Sample collection

Tissue was collected after identification of suitable patients through multi-disciplinary team case lists. Cancer tissue and corresponding normal colorectal tissue was collected.

Conventional light microscopy

H&E stained slides were used to understand tissue morphology.

Table 2: Tumour staging according to TNM8.

Adapted from Appendix A Royal College of Pathology Minimum Dataset, Used from December 2017.

(9)

pT	Primary tumour
pTX	Primary tumour cannot be assessed
pT0	No evidence of primary tumour
pT1	Tumour invades submucosa
pT2	Tumour invades muscularis propria
pT3	Tumour invades into subserosa or into non-peritonealised pericolic or perirectal tissues
pT4	Tumour perforates visceral peritoneum (4a) and/or directly invades other organs or structures (4b)
pN	Regional lymph nodes
pNX	Regional lymph nodes cannot be assessed
pN0	No regional lymph node metastatic disease
pN1	Metastatic disease in 1–3 regional lymph nodes pN1a: Metastasis in 1 regional lymph node pN1b: Metastases in 2–3 regional lymph nodes pN1c: Tumour deposit(s), i.e. satellites, *in the subserosa, or in non-peritonealised pericolic or perirectal soft tissue without regional lymph node metastatic disease (tumour deposits are ignored if there is nodal metastatic disease)
pN2	Metastatic disease in 4 or more regional lymph nodes pN2a: Metastases in 4–6 regional lymph nodes pN2b: Metastases in 7 or more regional lymph nodes *Tumour deposits, or satellites, are discrete macroscopic or microscopic nodules of cancer in the pericolorectal adipose tissue's lymph drainage area of a primary carcinoma that are discontinuous from the primary and without histological evidence of residual lymph node or identifiable vascular or neural structures.
pM	Distant metastatic disease pM1: Distant metastatic disease pM1a Metastasis confined to one organ without peritoneal metastases pM1b: Metastases in more than one organ pM1c: Metastases to the peritoneum with or without other organ involvement

Table 3: Details of the antibodies and lectin used in these methods.

Antibody/Lectin	Company	Dilution	Reference number	Techniques used for
Rabbit polyclonal wide-spectrum Cytokeratin antibody	Abcam	1:200	ab9377	Confocal and Light Sheet Microscopy
Monoclonal mouse anti-human cytokeratin, Clone AE1/3	DAKO	1:100	M3515	IHC
DAKO Flex CD31	DAKO	n/a	IR610	IHC
Monoclonal mouse anti-human CD31, endothelial cell clone	DAKO	1:20	M0823	IHC, Confocal and Light Sheet microscopy
Monoclonal mouse anti-human podoplanin clone D2:40	DAKO	1:100	M3619	IHC, Confocal and Light Sheet Microscopy
Lycopersicon Esculentum	Vector Laboratories	1:100	DL-1178	Confocal and Light Sheet Microscopy
AlexaFluor 647 donkey-anti mouse Ab	Invitrogen by Thermo Fisher Scientific	1:500	A31571	Confocal and Light Sheet Microscopy
AlexaFluor 647 donkey-antirabbit Ab	Invitrogen by Thermo Fisher Scientific	1:500	A-31573	Confocal and Light Sheet Microscopy
Mouse monoclonal anti-human MutL Protein Homolog 1. Clone ES05 (MLH1)	DAKO	n/a	IR079	IHC on reverse cleared tissue
Mouse monoclonal anti-human MutS Protein Homolog 2. Clone FE11 (MSH2)	DAKO	n/a	IR085	IHC on reverse cleared tissue
Mouse monoclonal anti-human MutS protein homolog 6. Clone EP49 (MSH6)	DAKO	n/a	IR086	IHC on reverse cleared tissue
Rabbit monoclonal Anti-human Postmeiotic Segregation Increased 2. Clone EP51 (PMS2)	DAKO	1:40	M3647	IHC on reverse cleared tissue

Immunohistochemistry of paraffin-embedded sections (IHC-P)

IHC was used to optimise our antibodies of interest.

Confocal microscopy

Used to assess antibody compatibility with immunofluorescence (IF) staining. Images are limited in depth and field of view but are extremely high resolution.

Light sheet microscopy

Tissue was prepared using multiple permeabilization solutions before immunolabelling. Sample were optically cleared before imaging. We followed an adapted iDISCO technique for these experiments (10).

Reverse Clearing

A proposed advantage to light sheet microscopy is the preservation of irreplaceable diagnostic material.

To rehydrate an optically cleared sample, it was moved through graded methanol with PBS (100%, 100%, 80%, 60%, 40%, 20%) for one hour each, with shaking. The sample was then washed within a 24hour period before being placed in 70% ethanol to be processed and paraffin embedded.

Autostainer procedure for deficient mismatch repair panel antibodies

Antibody staining on reverse cleared tissue was trialled using the Lynch Syndrome screening panel (MLH1, MSH2, MSH6 and PMS2).

Image processing for 3D analysis

3D image snapshots and mp4 video clips were made using Imaris software Version 9.2.4 (11). The software compiles the z-stack TIFF images taken on the light-sheet microscope itself and assembles them to show a 3D reconstruction of the sample.

Results

Epithelial staining

Cytokeratin was chosen as the epithelial marker in colorectal tissue (figure 3). This allowed visualisation of tumour tissue.

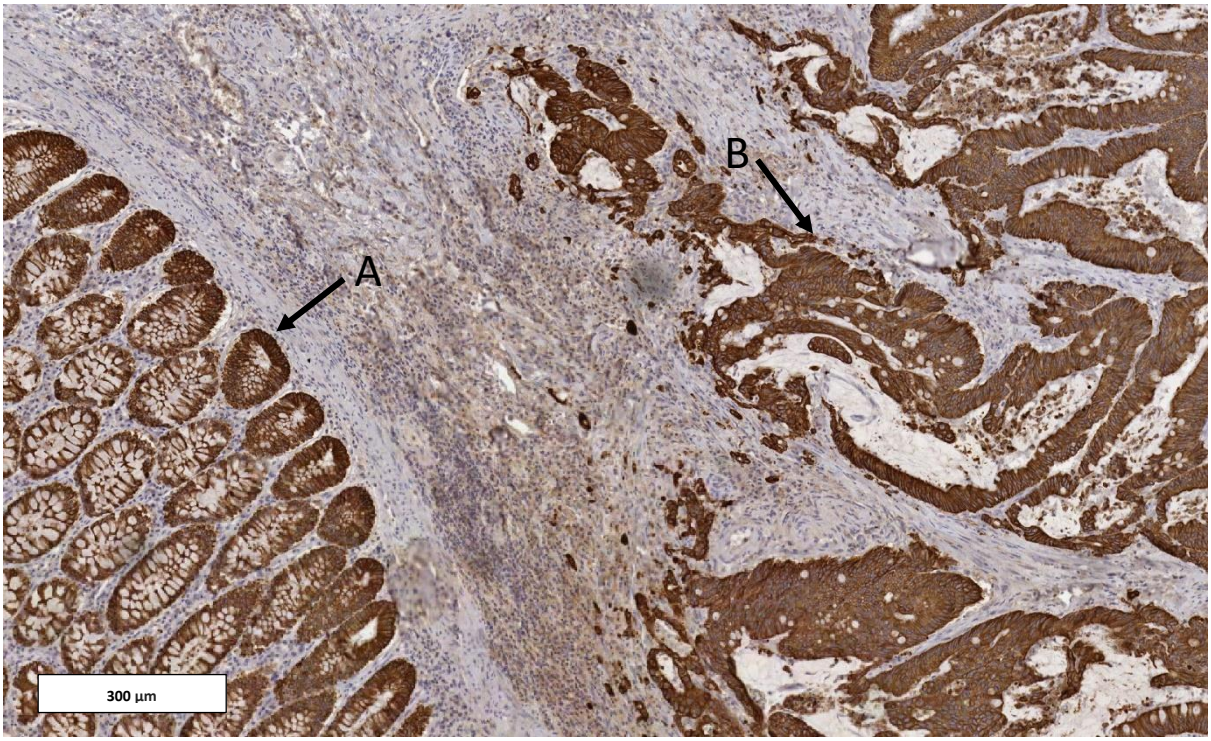

Figure 3. IHC staining using cytokeratin.

This image shows cytokeratin staining of normal epithelial staining (arrow A) and staining in tumour (arrow B). The image shows pale blue counterstain between these two areas.

Images from the confocal microscope showed clear staining of epithelial structures, there was little background staining (figure 4).

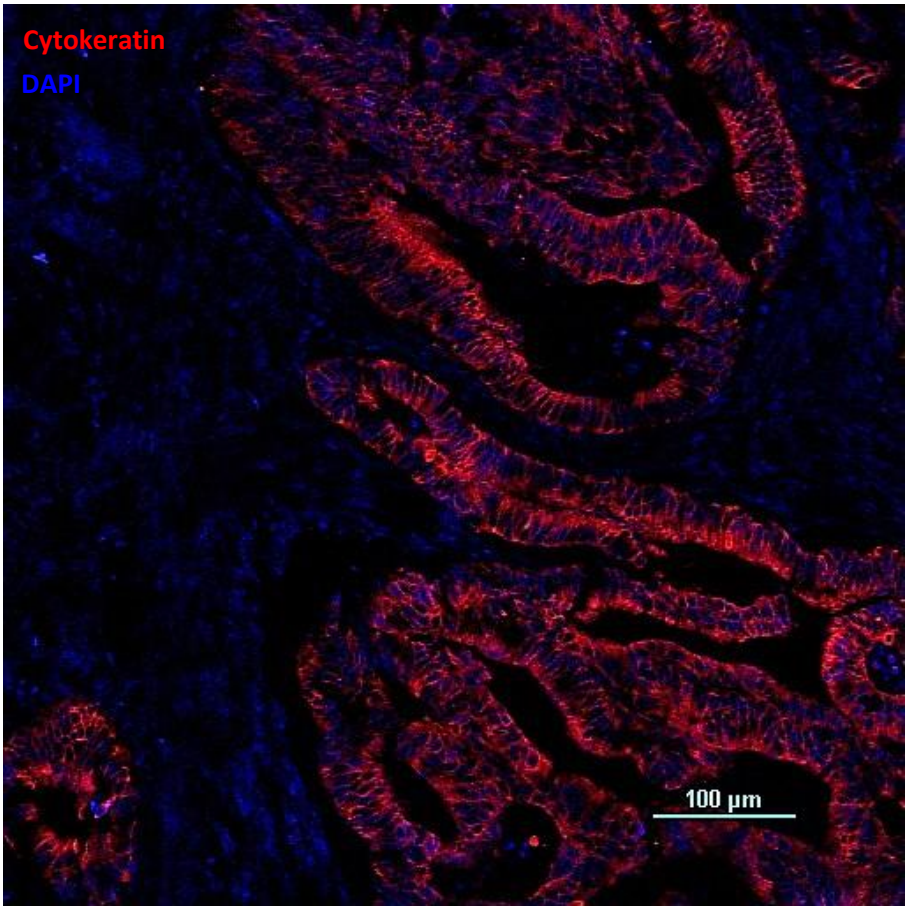

Figure 4: IF staining using cytokeratin.

This image shows the cytokeratin staining pattern in colorectal cancer. The blue staining is DAPI, a nuclear stain while the red colour is the cytokeratin stain.

Due to the clear staining achieved with this antibody we imaged areas of perineural invasion to visualise cancer progression alongside a nerve (figure 5). Imaging of the invading edge of cancer showed how small tumour cell groups can become detached from the main body of the tumour and invade further into the tissue (figure 5, arrow C).

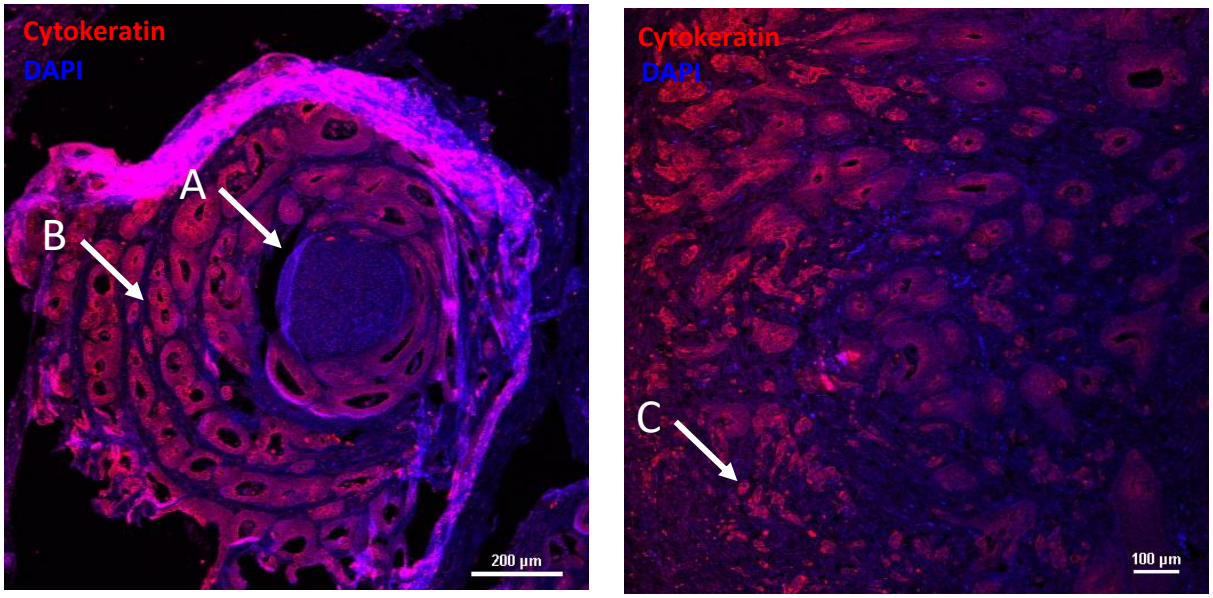

Figure 5: Further IF staining using cytokeratin.

The image on the left shows tumour (arrow B) growing around a nerve (arrow A). This is described as perineural invasion and shows a potential route cancer can use to further invade tissue. The image on the right shows the invading edge of the tumour including small areas which have become detached from the main tumour body and are able to grow further into the tissue (arrow C).

Cytokeratin was then used for light-sheet microscopy. The images showed limited, non-specific surface fluorescence restricted to the gastrointestinal submucosa (figure 6). The cytokeratin has not bound exclusively to epithelium but instead has clumped in and around the intestinal crypts. This requires further optimisation to provide useful data.

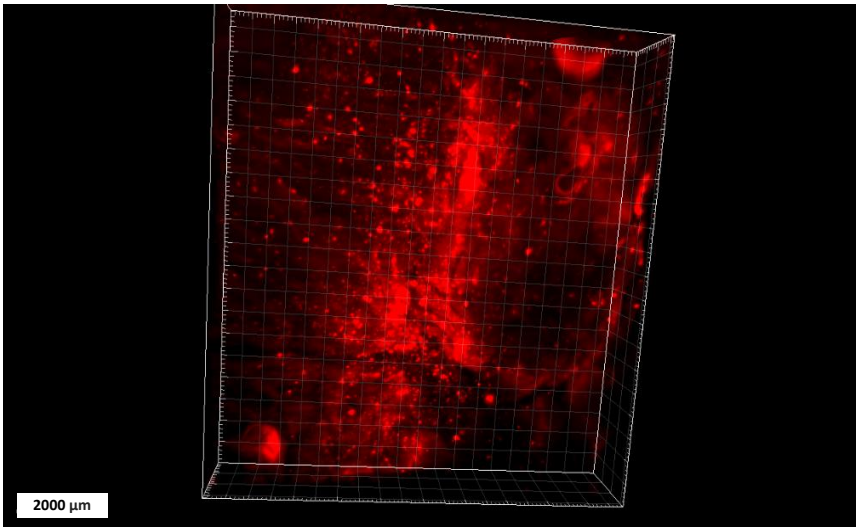

Figure 6: CRC sample stained with cytokeratin and imaged using light sheet microscopy

This figure shows a 3D reconstructed image using Imaris software. It shows poor cytokeratin staining.

Lymphatic staining

D2:40, an antibody to podoplanin was used to visualise lymphatic vasculature. IHC showed some detailed staining of lymphatic vasculature (figure 7, arrow A). However, we also saw some non-specific staining in areas of muscle (figure 8).

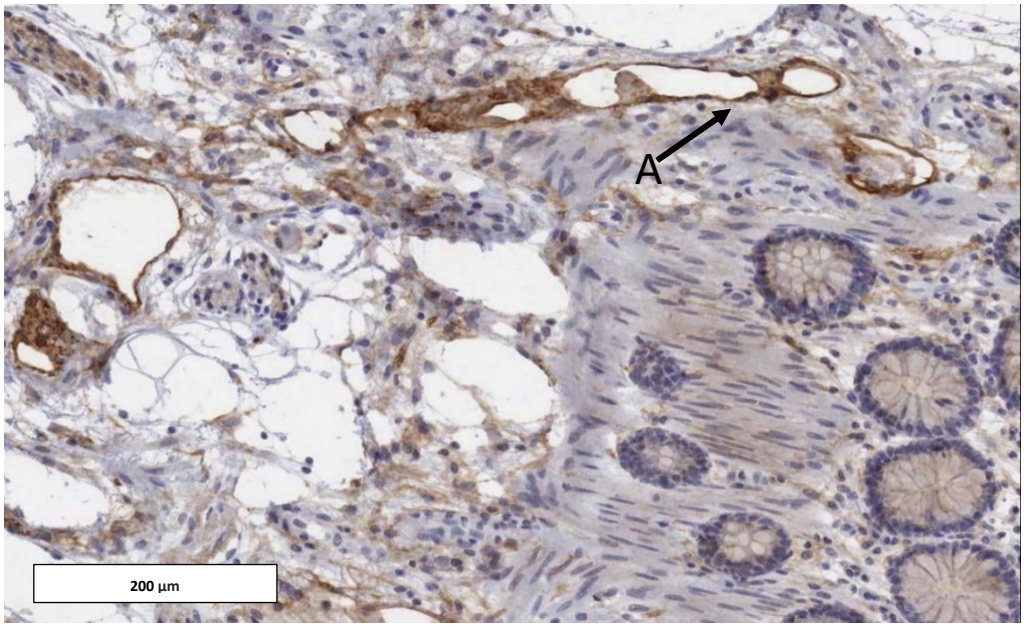

Figure 7: IHC staining using D2:40.

Image showing IHC staining of lymphatic vasculature (arrow A) using the D2:40 antibody.

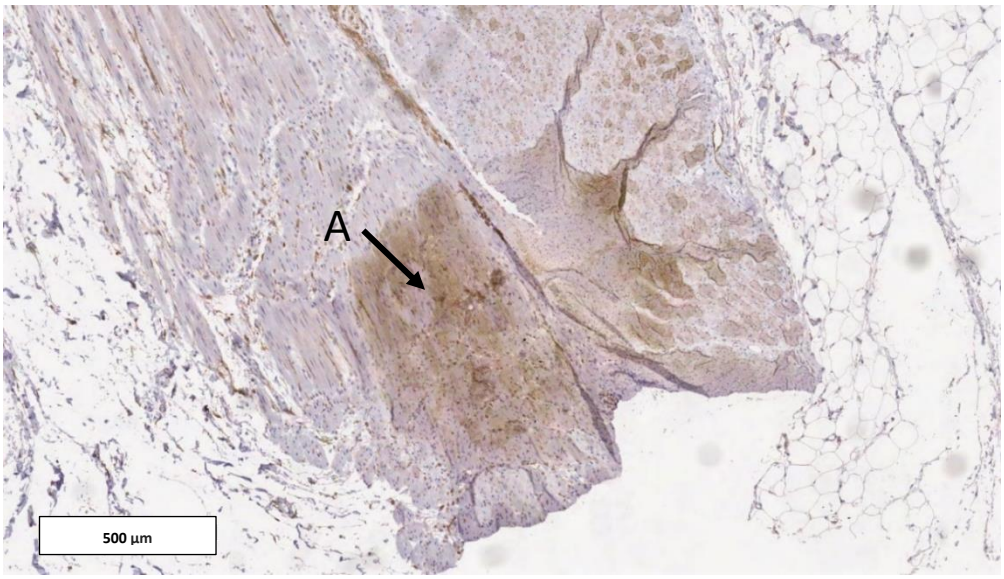

Figure 8: IHC staining using D2:40

Image showing areas of non-specific staining (arrow A) in muscle tissue when using the D2:40 antibody.

D2:40 was used on the confocal microscope. Staining appeared specific to lymphatic vasculature. A dual stain with the CD31 antibody to blood vessels was trialled and showed specific staining of the two antibodies in unison (figure 9).

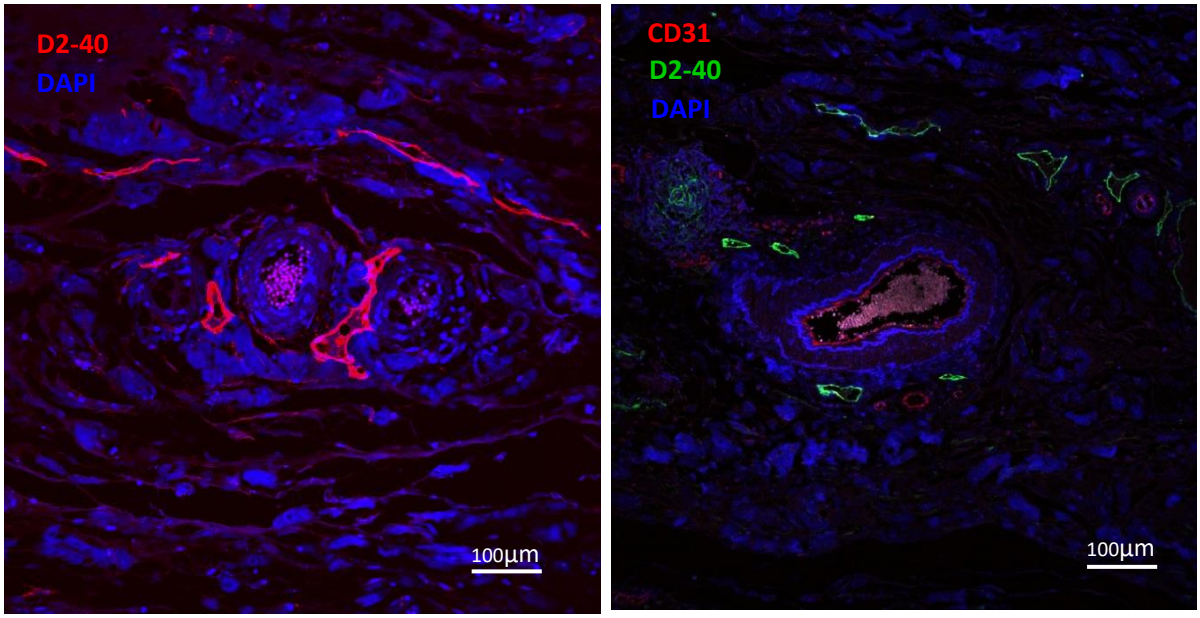

Figure 9: IF staining using D2:40.

The image on the left shows the D2:40 antibody staining lymphatic vessels (red) in normal colorectal tissue.

The image on the right shows the dual staining of D2:40 and CD31 in normal colorectal tissue.

Results from the light-sheet microscope using D2:40 were difficult to interpret. Obvious vessels (figure 10, arrow A) were shown in the images obtained but these appeared too large for lymphatic vasculature. The large number of vessels in the mucosa were mucosal capillaries. It is more likely the vessels seen in figure 10 are blood vessels.

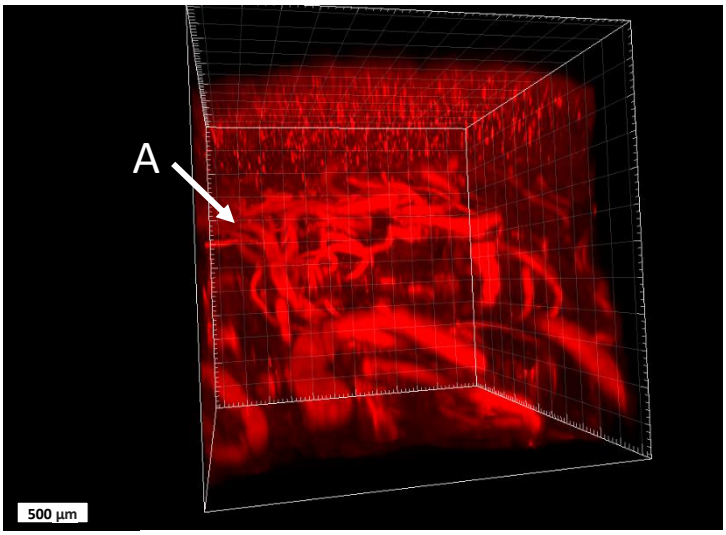

Figure 10: Light sheet microscopy image of staining using D2:40.

This image shows a 3D reconstructed image using Imaris software. It shows staining of large vessels (arrow A), these appear to be blood vessels, not lymphatic vasculature as expected.

Staining of blood vasculature

This project utilised both CD31 and LEL, a lectin, to visualise blood vessels.

IHC was performed using the CD31 antibody. Two variations of CD31 were used to compare staining between a ready-to-use (figure 10) and optimised (figure 11) antibody. Both antibodies produced specific, accurate staining of blood vessels. Experiments were continued using the optimised antibody.

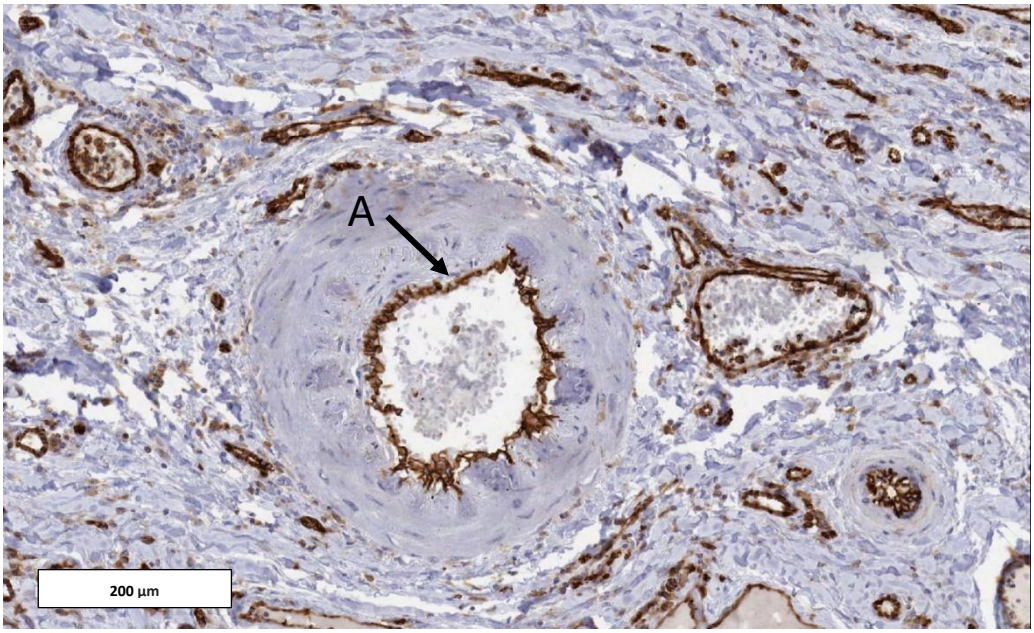

Figure 11: IHC staining using a ready-to-use CD31 antibody.

Arrow A indicates positive staining of a large, muscular blood vessel.

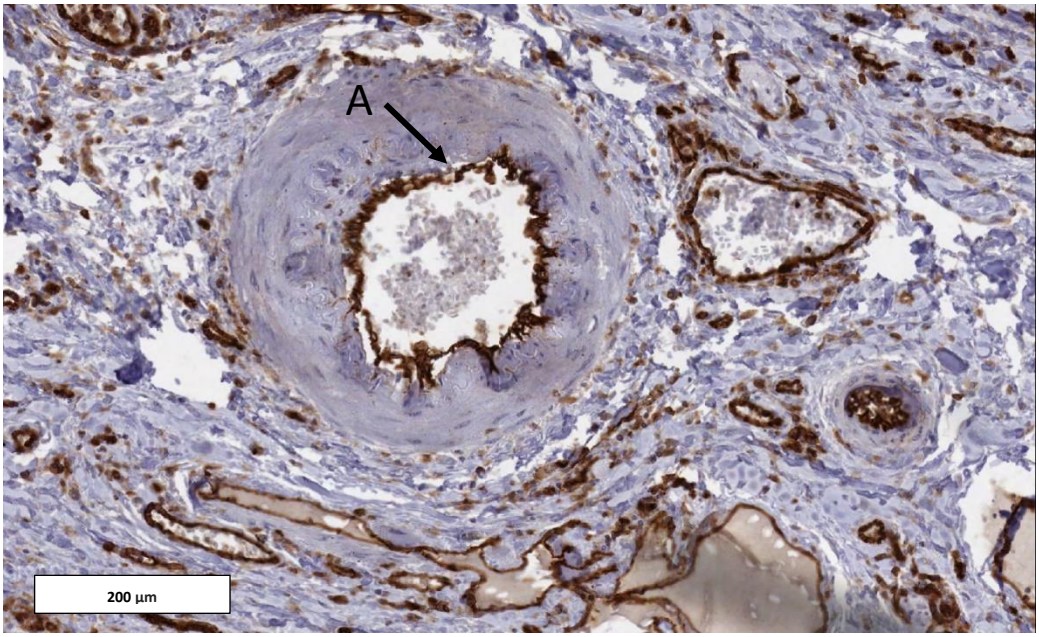

Figure 11: IHC staining using the optimised CD31 antibody at 1:20 dilution.

Arrow A indicates positive staining of a large, muscular blood vessel.

CD31 also provided accurate and specific staining of the blood vasculature using confocal microscopy.

The vessels visualised ranged from larger, muscular vessels to much smaller vessels, likely to be capillaries within the intestinal crypts. Figure 12 shows positive CD31 results using confocal microscopy alongside a negative control slide which was used in all experiments.

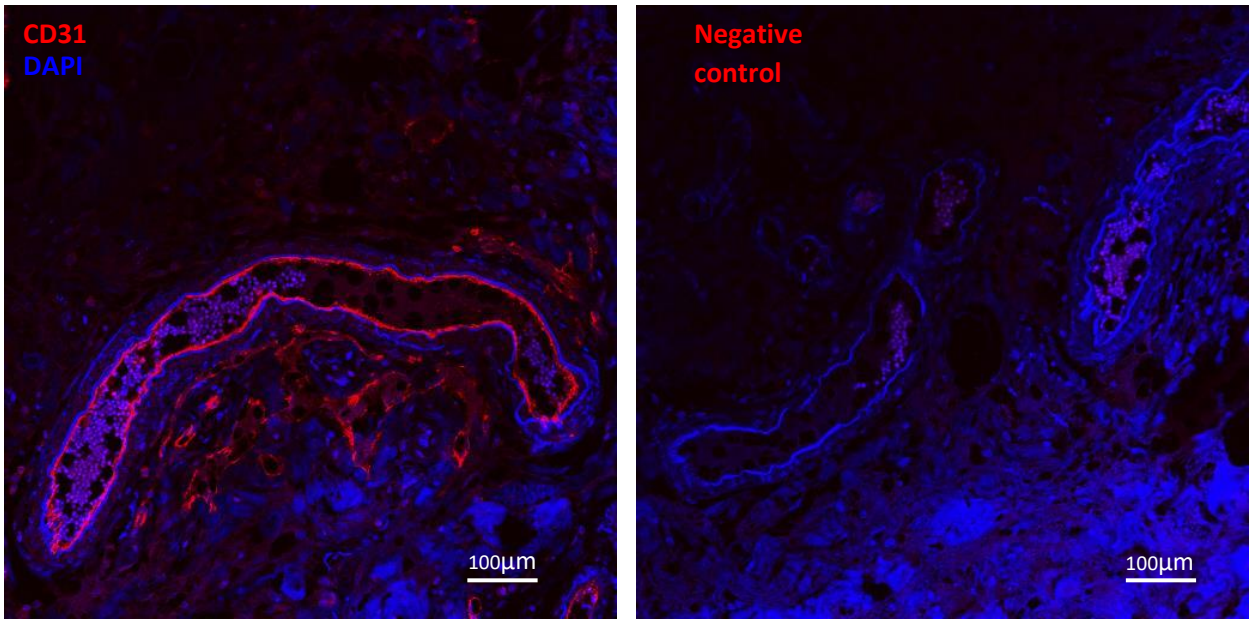

Figure 12: Immunofluorescence staining using CD31.

The image on the left shows clear staining of blood vessels in red alongside a nuclear (blue) stain. The image on the right shows the negative control tissue.

The CD31 antibody was used to stain optically cleared 3D for light-sheet microscopy. The images showed clear staining of vascular endothelium. Vessels were visualised in healthy tissue samples (figure 13, arrow A). We were also able to visualise blood vessels in cancer samples (figure 14). Cancer samples showed the presence of some smaller, micro-vessels not seen in normal, healthy tissue (figure 14, arrow A). More distortion is seen in the cancer sample due to difficulties with optical clearing and antibody penetration.

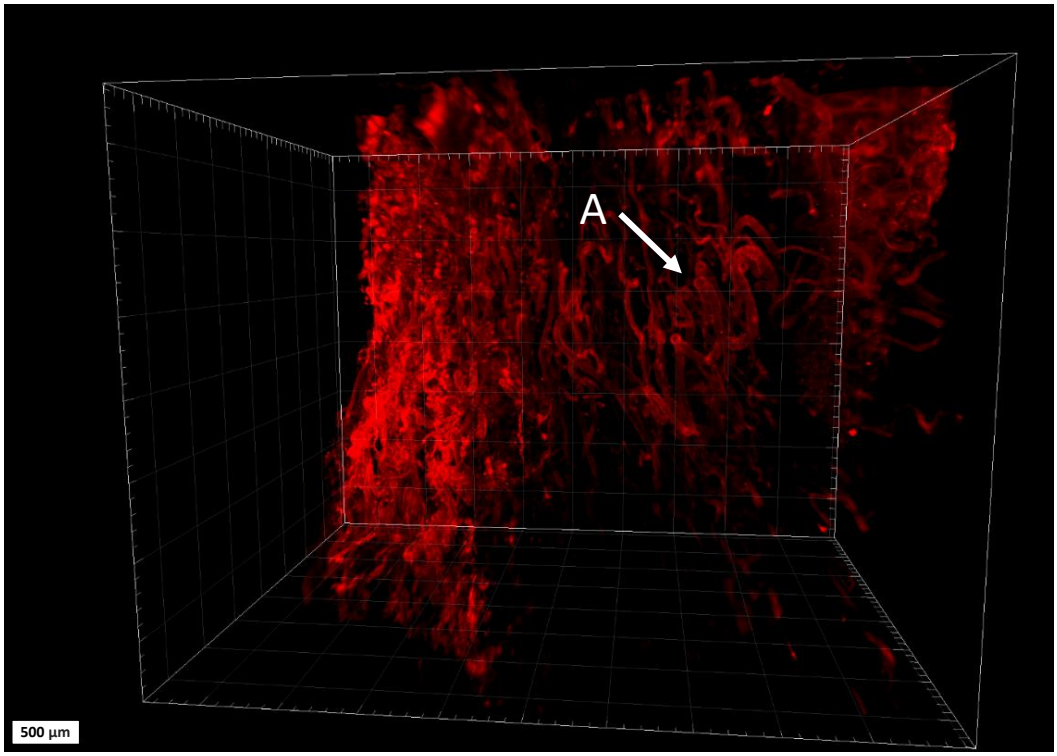

Figure 13: CD31 staining using light-sheet microscopy.

This image shows clear staining of 3D blood vasculature in healthy colorectal tissue.

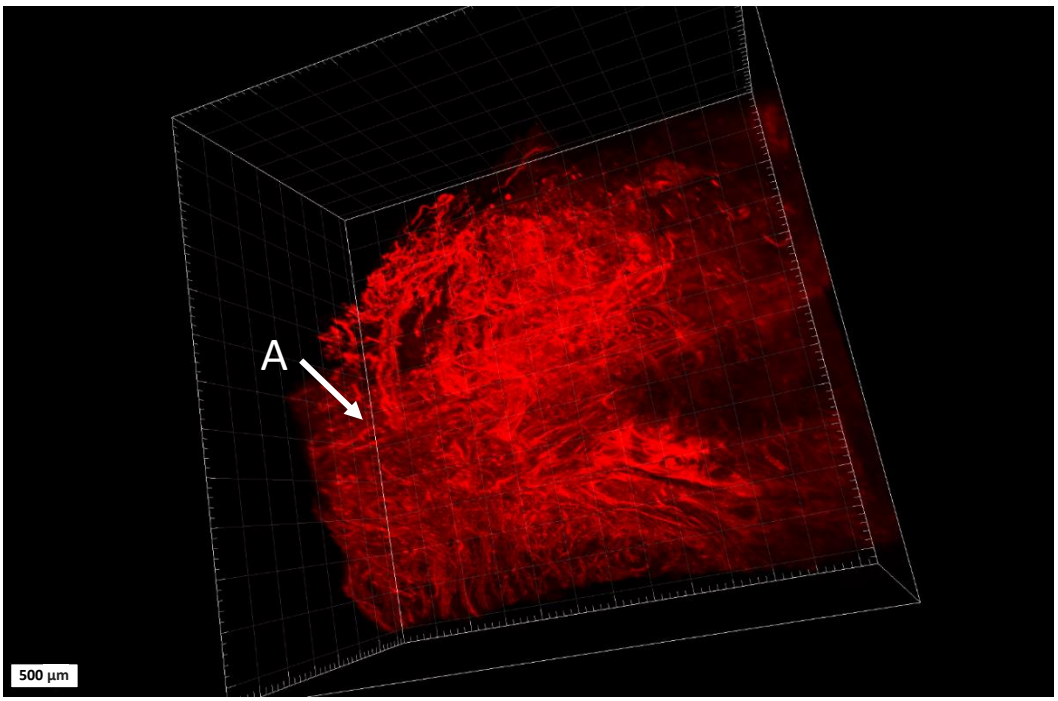

Figure 14: CD31 staining using light-sheet microscopy.

This image shows CD31 staining of CRC tissue in 3D.

LEL is pre-conjugated with a fluorophore. This was used to shorten the preparation process of light-sheet samples. Optimisation using IF staining showed crisp staining of the vasculature with little background fluorescence.

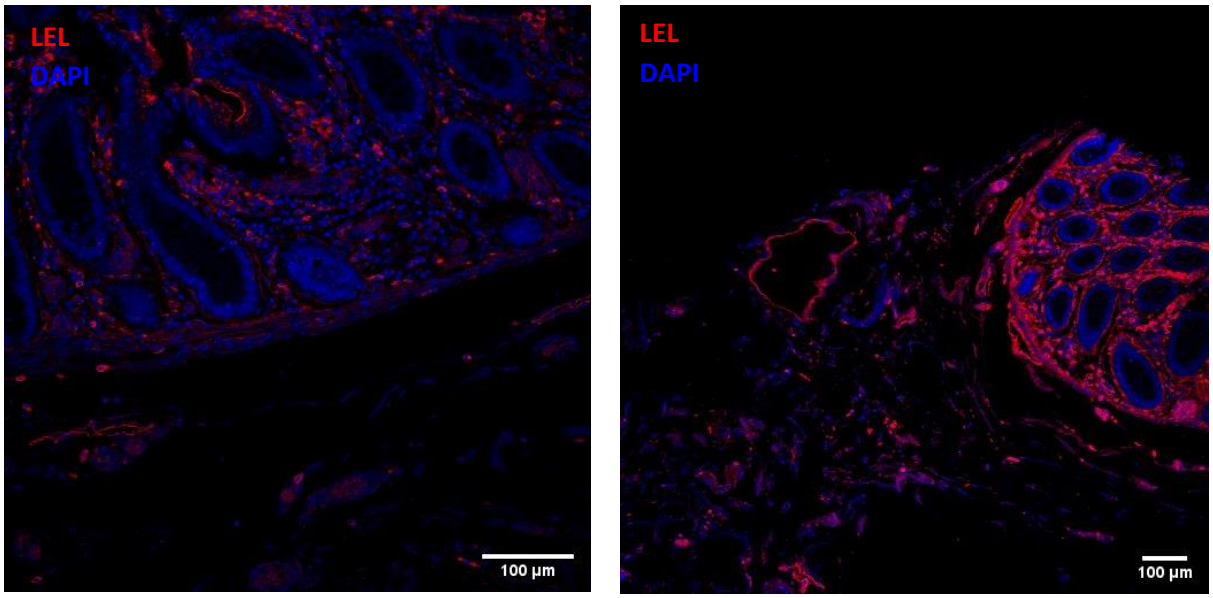

Figure 15: Immunofluorescence staining using LEL.

Images show blood vessel staining in normal colorectal tissue using LEL.

Imaging on the light-sheet microscope showed crisp staining of blood vessels with less background fluorescence compared to the antibody stained samples (figure 16).

As seen with the CD31 antibody the penetration of the lectin through the sample was less complete in cancer samples (figure 17).

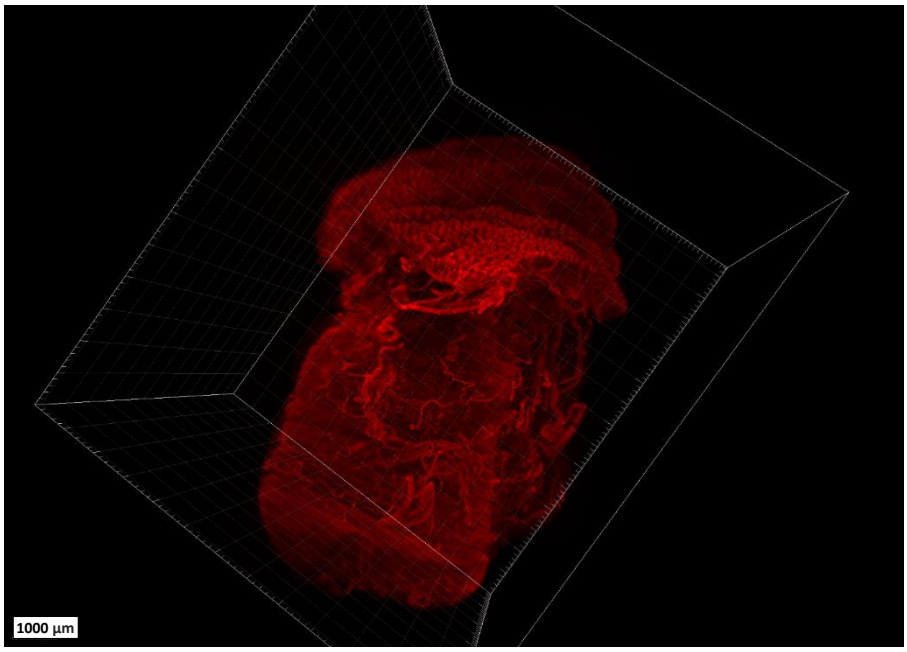

Figure 16: LEL staining using light-sheet microscopy.

This image shows an Imaris reconstructed image of normal colorectal tissue stained with LEL. This shows specific staining of the tissue vasculature with little background fluorescence.

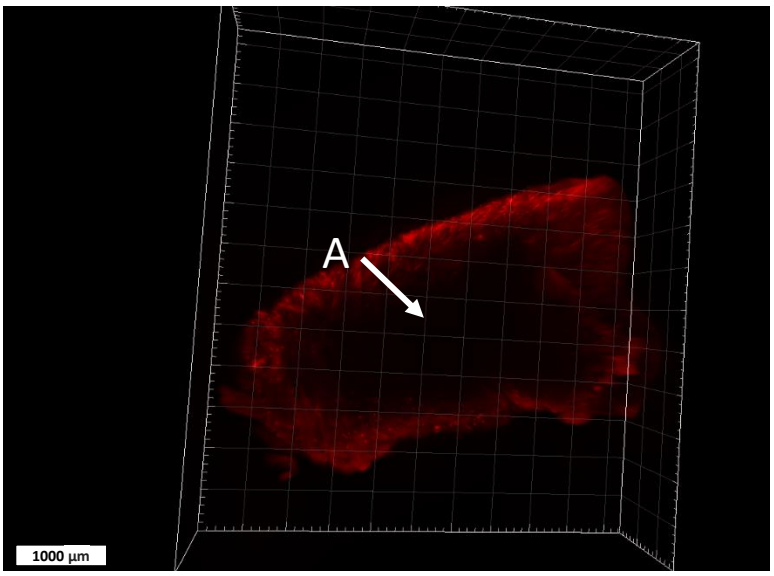

Figure 17: LEL staining using light-sheet microscopy.

This image shows LEL staining on tumour tissue. This staining does not penetrate the tissue sample completely leaving areas in the middle of the tissue unstained.

Reverse Optical Clearing

As this project aims to evaluate the use of light-sheet microscopy as an investigative technique it was important to ascertain whether the tissue could undergo conventional testing after it had been optically cleared and imaged on the light-sheet microscope.

H&E staining of a reverse cleared sample showed clear preservation of the tissue morphology (figure 18).

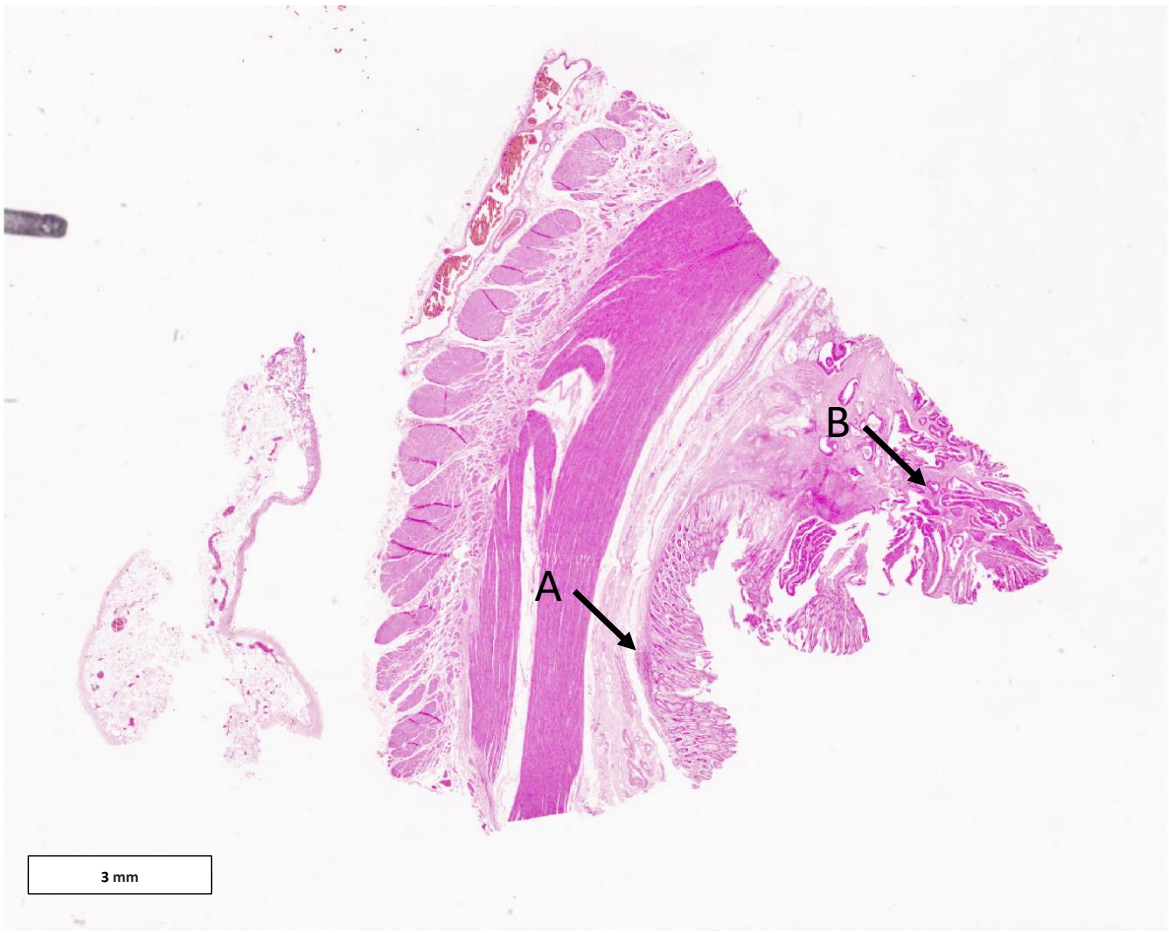

Figure 18: H&E staining on a reverse cleared sample.

This image shows H&E staining of colorectal tissue. This tissue sample that has undergone optical clearing which has been reversed before H&E staining. Arrow A indicates healthy, normal mucosa whereas arrow B shows tumour tissue. This is a pT2 cancer.

This reverse cleared tissue was then stained using established antibodies routinely used for Lynch syndrome screening (MLH1, MSH2, MSH6 and PMS-2). The results show staining as expected when using each antibody from the Lynch syndrome screening panel. Figure 19 shows staining, as expected using PMS-2.

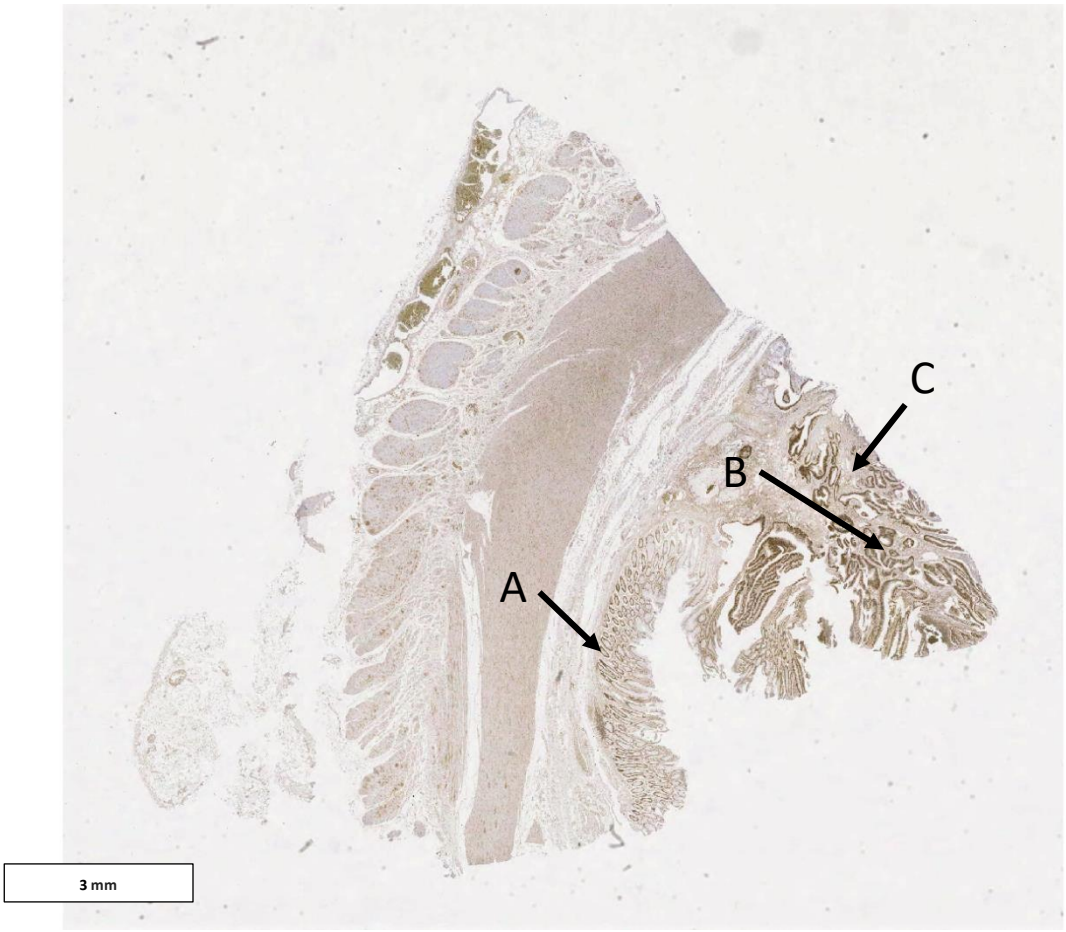

Figure 19: IHC staining using PMS-2

This image shows a reverse cleared tissue section after IHC staining with a PMS-2 antibody. The staining seen in this sample is as expected for this antibody. Arrow A indicates healthy, normal mucosa whereas arrow B shows tumour tissue. Arrow C shows a positive internal control with staining of the lymphocytes. This is a pT2 cancer.

Discussion

Epithelial staining: Cytokeratin

Results from this project have shown positive cytokeratin staining using IHC and IF techniques. Contrary to our expectations, specific cytokeratin staining was not transferable to the light-sheet microscopy protocol.

Further optimisation of the clearing technique is required to provide more informative staining. 3D reconstruction of the human colon has been carried out by Neckel et al. using a similar wide-spectrum cytokeratin to the one used in this project alongside several other epithelial markers. This may explain how they gained more complete and specific epithelial staining. They also used a different clearing mechanism, called CLARITY (12).

Lymphatic staining: D2:40

Lymphatic invasion is the most important predictive factor for LNM in early colorectal cancer (13). LNM is an important mechanism of disease spread and progression in colorectal cancer. Due to problems within the optimisation process of our D2:40 antibody we were not able to reproduce the specific IHC staining patterns seen in previous studies (14), (6). One possible explanation could be the differences in tissue fixation before our experiments began or the use of cancer associated normal tissue.

Staining of blood vasculature: LEL

The use of LEL decreased the preparation time of 3D tissue from 24 to ten days. Using a pre-conjugated blood vessel marker reduced incubation time and problems associated with non-specific staining of our fluorophore bound secondary antibody reducing sample background staining.

Staining of tumorous samples proved suboptimal using LEL and CD31 as incomplete sample penetration was seen.

Tanaka et al. successfully used the iDISCO clearing technique with methanol pre-treatment in their study of bladder tumours (15). The use of the methanol pre-treatment protocol may provide better clearing for tumour samples than the method used in this project (10).

Staining of blood vasculature: CD31

In the tumours that we could image there was evidence of changed vasculature. More numerous micro-vessels were seen in tumour tissue. Tumour angiogenesis is crucial to cancer progression and survival as it grows, therefore it is likely that the small vessels we have seen are newly formed vessels of smaller diameter. The density of these micro-vessels has been proposed as a prognostic indicator in early CRC (16), (17), (18).

Reverse optical clearing

The present results are significant in at least two major respects. First the H&E stained sections showed remarkably unchanged tissue morphology in the normal tissue as well as the areas of CRC. Secondly IHC of the same sample showed successful staining for multiple antibodies.

Limitations

The light-sheet microscope is currently a research method due to it's cost and lack of studies demonstrating it's benefit.

A major limitation is the time required to collect data.

Variation of results could impact future routine use of this technique. Sample to sample variability occurred throughout the study, including samples prepared together, this inconsistency could make light-sheet microscopy incompatible with routine clinical work.

Future work

Optimisation of a more reliable and accurate lymphatic stain is important if this technique is ever to be clinically useful.

Antibodies such as the LYVE-1 antibody used by Tanaka et al. to stain bladder tumours could be trialled in colorectal tissue (15).

To determine if this technique could be superior to previous digital pathology techniques (6) a direct comparison of the two techniques should be undertaken.

Conclusion

This project has shown that tissue investigated through light-sheet microscopy can visualised in 3D and then subsequently analysed by routine diagnostic techniques. As a new technique there is still further optimisation required to attain reliable optical clearing and staining through healthy and tumorous colorectal tissue.

Acknowledgements

Thank you to my supervisors Professor Philip Quirke and Dr Scarlet Brockmoeller. Thank you also to Gemma Hemmings and Ruth Hughes for their technical assistance.

Thank you to The Pathological Society for their generous sponsorship of this project.

TOTAL WORD COUNT: 1,995 words

References

1. Bhangu A, Brown G, Nicholls RJ, Wong J, Darzi A, Tekkis P. Survival outcome of local excision versus radical resection of colon or rectal carcinoma: a Surveillance, Epidemiology, and End Results (SEER) population-based study. Ann Surg. 2013 Oct;258(4):563–9; discussion 569-571.

2. Office for National Statistics. Cancer registration statistics, England - Office for National Statistics [Internet]. 2016 [cited 2018 Oct 27]. Available from: https://www.ons.gov.uk/peoplepopulationandcommunity/healthandsocialcare/conditionsanddiseases/bulletins/cancerregistrationstatisticsengland/final2016

3. World Cancer Research Fund. Colorectal cancer statistics [Internet]. World Cancer Research Fund. 2018 [cited 2019 May 23]. Available from: https://www.wcrf.org/dietandcancer/cancer-trends/colorectal-cancer-statistics

4. Cancer Research UK. TNM Staging | Bowel Cancer | Cancer Research UK [Internet]. 2018 [cited 2019 Feb 28]. Available from: https://www.cancerresearchuk.org/about-cancer/bowel-cancer/stages-types-and-grades/TNM-staging

5. Morris EJA, Whitehouse LE, Farrell T, Nickerson C, Thomas JD, Quirke P, et al. A retrospective observational study examining the characteristics and outcomes of tumours diagnosed within and without of the English NHS Bowel Cancer Screening Programme. Br J Cancer. 2012 Aug 21;107(5):757–64.

6. Brown PJ, Toh E-W, Smith KJE, Jones P, Treanor D, Magee D, et al. New insights into the lymphovascular microanatomy of the colon and the risk of metastases in pT1 colorectal cancer obtained with quantitative methods and three-dimensional digital reconstruction. Histopathology. 2015 Aug 1;67(2):167–75.

7. Toh E-W, Brown P, Morris E, Botterill I, Quirke P. Area of submucosal invasion and width of invasion predicts lymph node metastasis in pT1 colorectal cancers. Dis Colon Rectum. 2015 Apr;58(4):393–400.

8. Santi PA. Light Sheet Fluorescence Microscopy: A Review. Journal of Histochemistry and Cytochemistry. 2011 Feb;59(2):129.

9. Royal College of Pathologists. Cancer datasets and tissue pathways [Internet]. 2018 [cited 2018 Nov 12]. Available from: https://www.rcpath.org/profession/guidelines/cancer-datasets-and-tissue-pathways.html

10. Renier N, Wu Z, Simon DJ, Yang J, Ariel P, Tessier-Lavigne M. iDISCO: a simple, rapid method to immunolabel large tissue samples for volume imaging. Cell. 2014 Nov 6;159(4):896–910.

11. Bitplane. Imaris. Zurich, Switzerland;

12. Neckel PH, Mattheus U, Hirt B, Just L, Mack AF. Large-scale tissue clearing (PACT): Technical evaluation and new perspectives in immunofluorescence, histology, and ultrastructure. Scientific Reports. 2016 Sep 29;6:34331.

13. Bosch SL, Teerenstra S, de Wilt JHW, Cunningham C, Nagtegaal ID. Predicting lymph node metastasis in pT1 colorectal cancer: a systematic review of risk factors providing rationale for therapy decisions. Endoscopy. 2013 Oct;45(10):827–34.

14. Smith KJE, Jones PF, Burke DA, Treanor D, Finan PJ, Quirke P. Lymphatic Vessel Distribution in the Mucosa and Submucosa and Potential Implications for T1 Colorectal Tumors. Dis Colon Rectum. 2011 Jan;54(1):35–40.

15. Tanaka N, Kaczynska D, Kanatani S, Sahlgren C, Mitura P, Stepulak A, et al. Mapping of the three-dimensional lymphatic microvasculature in bladder tumours using light-sheet microscopy. British Journal of Cancer. 2018 Apr;118(7):995–9.

16. Tomisaki S, Ohno S, Ichiyoshi Y, Kuwano H, Maehara Y, Sugimachi K. Microvessel quantification and its possible relation with liver metastasis in colorectal cancer. Cancer. 1996;77(8):1722–8.

17. Guetz GD, Uzzan B, Nicolas P, Cucherat M, Morere J-F, Benamouzig R, et al. Microvessel density and VEGF expression are prognostic factors in colorectal cancer. Meta-analysis of the literature. British Journal of Cancer. 2006 Jun;94(12):1823.

18. Rajaganeshan R, Prasad R, Guillou PJ, Chalmers CR, Scott N, Sarkar R, et al. The influence of invasive growth pattern and microvessel density on prognosis in colorectal cancer and colorectal liver metastases. British Journal of Cancer. 2007 Apr;96(7):1112–7.